Nanoscale

RSC Publishing

PAPER

Quantitative analysis of dendron-conjugated cisplatin-complexed gold nanoparticles using scanning particle mobility mass spectrometry†

Cite this: *Nanoscale*, 2013, **5**, 5390

De-Hao Tsai, Tae Joon Cho, Sherrie R. Elzey, Julien C. Gigault and Vincent A. Hackley*

We report a high-resolution and traceable method to quantify the drug loading on nanoparticle-based cancer therapeutics, and demonstrate this method using a model cisplatin functionalized dendron–gold nanoparticle (AuNP) conjugate. Electrospray differential mobility analysis (ES-DMA) provides upstream size classification based on the electrical mobility of AuNP conjugates in aerosol form following electrospray conversion from the aqueous suspension. A condensation particle counter (CPC) and inductively coupled plasma mass spectrometer (ICP-MS) provide the principal downstream quantification. CPC and ICP-MS yield complementary number-based and elemental mass-based particle size distributions, respectively. Conjugation using three different dendron formulations was differentiated based on changes in the mean mobility particle size. The subsequent cisplatin complexation to the dendron conjugates was quantified by coupling ES-DMA with ICP-MS. Discrete AuNP clusters (*e.g.*, dimers, trimers) could be resolved from the relative quantity of atoms (*i.e.*, Au and Pt) per particle after separation by ES-DMA. Surface density of cisplatin on Au was shown to be proportional to the density of carboxylic groups present and was independent of the state of AuNP clustering. Additionally, we found that colloidal stability of the conjugate is inversely proportional to the surface loading of cisplatin. This study demonstrates a prototype methodology to provide traceable quantification and to determine other important formulation factors relevant to therapeutic performance.

Received 30th January 2013
Accepted 11th April 2013

DOI: 10.1039/c3nr00543g

www.rsc.org/nanoscale

1 Introduction

Gold nanoparticles (AuNPs), surface engineered to carry the pharmacophore *cis*-diamminedichloroplatinum(II), also known as cisplatin‡ and denoted here as Pt^{II}, are attractive vectors for targeted cancer therapy.[1,2] In addition to the known potency in chemo-therapeutics, external radiation synchronized with the traditional Pt^{II}-based treatment has proven to be useful for inducing additional DNA damage and interfering with the DNA-repair process following radiation treatment.[3,4] Moreover, the "radiation-therapeutic" effect of Pt^{II} can be further enhanced through its combination with a AuNP vector. Beyond the well-known drug carrier functionality,[2,5–12] the capacity for AuNPs to deliver additional radiation dose to the cellular organelles by emitting Auger-like electrons is promising. The highly localized energy release from AuNPs can induce further damage to the targeted cells with high selectivity due to passive or active targeting.[2,13,14]

Although cisplatin-complexed AuNPs (Pt^{II}–AuNPs) provide a promising synergetic strategy for tumor treatment, an obvious challenge is to accurately engineer this nanoplatform on demand to achieve desired biological functionality. The therapeutic performance of Pt^{II}–AuNPs is dominated by the effective Pt^{II} dose, the conjugate stability, and the capacity to release Pt^{II} under acidic conditions.[2] Therefore, understanding the surface chemistry and choosing suitable formulations in the manufacturing process is of crucial importance for Pt^{II}–AuNP nanoplatforms. The overall therapeutic performance can be further improved conceptually by incorporating intelligent and complementary design principles.[7,11,15]

In this context, we turn to dendrons, which are highly uniform branching structures coupled to a single reactive functional unit.[16–20] Thiolated dendrons chemically bind to the AuNP surface, where the dendron corona provides dimensional control, functionality, hydrophilicity and steric repulsion (necessary to support colloidal stability of the conjugate in biological media).[19,21] Moreover, the dendron–AuNP conjugate can be designed to optimize functionality and stability for a specific application or set of conditions.[16,17,20] By choosing thiolated dendron ligands with suitable functional end-groups, in this case carboxylic acids,[1,2] the dendron–AuNP conjugate

Materials Measurement Science Division, National Institute of Standards and Technology, 100 Bureau Drive, Mail Stop 8520, Gaithersburg, MD 20899, USA. E-mail: vince.hackley@nist.gov

† Electronic supplementary information (ESI) available: Experimental procedures, instrumentation, materials and calculations. See DOI: 10.1039/c3nr00543g

‡ The identification of any commercial product or trade name does not imply endorsement or recommendation by the National Institute of Standards and Technology.

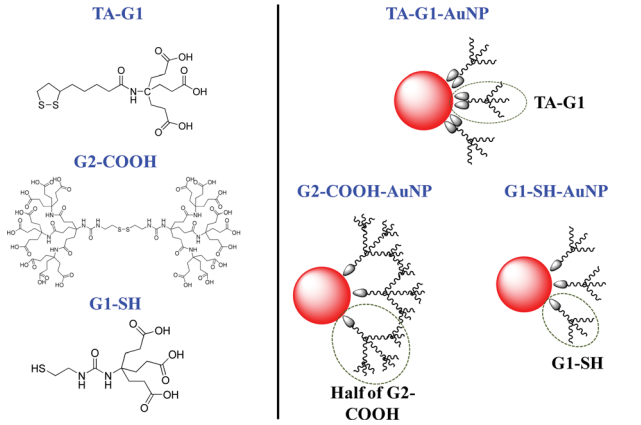

Fig. 1 Schematic illustration of unbound dendron ligands (left) and corresponding dendron–AuNP conjugates (right).[19] Here TA is thioctic acid, G is the generation number of the dendron and SH is the free thiol group.

complexes Pt^{II} to form the Pt^{II}–dendron–AuNP structure as a model chemo-radiation therapeutic agent.

The objectives of the present study were two-fold: (1) to develop an alternative and facile route to synthesize a stable cisplatin functionalized AuNP vector as a potential chemo-radiation therapeutic agent with desired Pt^{II} loading, and (2) using this model therapeutic agent, to develop and demonstrate a new high-resolution *in situ* method for size-resolved quantification of the therapeutic payload (cisplatin) in conjunction with size and stability characterization. The method described herein combines electrospray differential mobility analysis (ES-DMA) coupled with a condensation particle counter (CPC) and an inductively coupled plasma mass spectrometer (ICP-MS). We begin this study with the synthesis of three different structural forms of thiolated dendron ligands, denoted TA-G1, G1-SH, and G2-COOH (see Fig. 1). The ligands are subsequently conjugated to AuNPs (denoted as TA-G1–AuNP, G1-SH–AuNP, and G2-COOH–AuNP, respectively). Due to differences in chemical structure (*i.e.*, number of carboxylic groups per dendron) and surface density (*i.e.*, number of dendron ligands per unit surface area of Au),[19] the number of sites available for Pt^{II}-binding will differ for the three conjugates. Through the characterization of physical size, particle mass, and elemental composition, we quantify the effect of dendron structure on the Pt^{II} loading and colloidal stability of the model therapeutic agent, while demonstrating the overall efficacy of the proposed method.

2 Experimental section

2.1 Chemicals and materials

Cis-diamminedichloroplatinum(II) (trade name cisplatin; formula *cis*-$PtCl_2(NH_3)_2$) and silver nitrate ($AgNO_3$, 99%) were purchased from Aldrich Chemical Co. (St. Louis, MO). Sodium hydroxide (NaOH, pellets, 99%) was obtained from Mallincrodt Chemicals (Phillipsburg, NJ). All chemicals were used without further purification. In the initial step, aqueous solutions of cisplatin (2.5 mmol L^{-1}) and $AgNO_3$ (5 mmol L^{-1}) were combined (1 : 1) and stirred in the dark, at room temperature for 12 h. A white precipitate (AgCl) was filtered and the final concentration of cisplatin (with Cl^- displaced by the more labile NO_3^-) was adjusted to 1.25 mmol L^{-1}.

To formulate carboxylate terminated dendron stabilized AuNP conjugates, previously reported dendrons were used as the starting material.[19] TAG1-COONa or G1-SH-COONa (500 μL, 2.5 mmol L^{-1} in 7.5 mmol L^{-1} NaOH or 5 mmol L^{-1} in 15 mmol L^{-1} NaOH, respectively) was added dropwise to a AuNP suspension (5 mL, ≈50 μg mL^{-1}, Ted Pella Inc., Redding, CA) and stirred for 5 h at room temperature. The resulting product was purified by centrifugal filtration fitted with a regenerated cellulose membrane [molecular mass cut-off (MMCO) = 100 kDa]. G2-COONa (500 μL, 2.5 mmol L^{-1} in 45 mmol L^{-1} NaOH) was added to the AuNP suspension in increments of 100 μL every 30 min, and stirred for 5 h (overall) at room temperature. The final product, G2-COOH–AuNP conjugates, were purified by centrifugal filtration (MMCO = 100 kDa).

To formulate the Pt^{II}–dendron–AuNP conjugates, 5 mL of dendron–AuNP suspension was added dropwise to a solution of *cis*-$[Pt^{II}(NH_3)_2(H_2O)_2](NO_3)_2$ (5 mL, 12.5 μmol L^{-1}) and stirred in the dark, at room temperature for 12 h. After reaction, the mixture was purified by dialysis (MMCO = 500 Da, cellulose ester membrane) against de-ionized water for two days.

2.2 Coupled scanning particle mobility mass spectrometry

The ES (model 3480, TSI, Inc., Shoreview, MN) generates an aerosol of nanoparticles by moving a liquid dispersion containing nanoparticles through a capillary (40 μm tip), where the droplets are sprayed under an electric field into a stream of dry air. The aerosolized nanoparticle stream is then carried into the DMA (model 3085, TSI, Inc.), and their size is classified based on electrical mobility under an applied DC electric field. The trajectory of a charged particle within the DMA column is directly related to the particle mobility diameter, $d_{p,m}$. As the voltage applied to the DMA is varied, particles of a specific $d_{p,m}$ exit the DMA and are detected by the CPC (model 3776, TSI, Inc.). In this study, the DMA and CPC were controlled using a custom LabView program (National Instruments Corp., Austin, TX). The ES-DMA-CPC was used to obtain a number-based particle size distribution (PSD, number concentration of particles in the gas phase, $N_{p,g}$, *versus* $d_{p,m}$). A step size of 0.2 nm was used to scan through the PSD in the ES-DMA-CPC, and the time interval between each step size was set 10 s.[22]

An ICP-MS (7700x, Agilent Technologies, Santa Clara, CA) was used to monitor ^{197}Au and ^{195}Pt. To couple the ES-DMA with the ICP-MS *via* a gas exchange device (GED), the exit sample flow of the DMA was connected to the GED inlet, and the GED outlet was directly connected to the ICP-MS torch. Details of this arrangement are provided in a previous publication.[22] Particles exiting the DMA were thus transported directly to the ICP-MS, and the ICP-MS was set to time-resolved acquisition (TRA) mode in order to monitor ^{197}Au and ^{195}Pt signal intensities as the DMA voltage increased. This procedure allows particles of a specific size to exit the DMA at each voltage step (*i.e.*, $d_{p,m}$ is a function of scanning time recorded by the TRA program) and to

be detected by the ICP-MS. Using this coupled ES-DMA-ICP-MS instrument, we obtained element-specific (*i.e.*, ^{197}Au or ^{195}Pt) elemental mass-based PSDs. In order to ensure proper performance, prior to initializing TRA mode the system was first tuned by using samples of Au colloid with a nominal diameter of 30 nm at concentrations of ≈48 μg mL^{-1}. Step size used for measurements in the ES-DMA-ICP-MS configuration was 0.2 nm, and the scanning time interval between each step size was 20 s. The absolute counts per second (cps) of ^{197}Au [$N_{\mathrm{Au(cps)}}$] and ^{195}Pt [$N_{\mathrm{Pt(cps)}}$] signals were subtracted from the baseline value. Using a spherical approximation for the AuNPs, the surface density of Pt^{II}, σ_{Pt} (*i.e.*, the number of Pt^{II} per unit Au surface area), can be calculated using eqn (1),

$$\sigma_{\mathrm{Pt}} = \frac{N_{\mathrm{Pt(cps)}}}{S_{\mathrm{AuNP(cps)}}} = \frac{N_{\mathrm{Pt(cps)}}}{N_{\mathrm{AuNP(cps)}} \times \pi {d_{\mathrm{p,0}}}^2}, \quad (1)$$

where $S_{\mathrm{AuNP(cps)}}$ is the ICP-MS measured surface area (derived from cps signal) and $d_{\mathrm{p,0}}$ is the diameter of bare AuNPs (*i.e.*, without surface conjugation). Assuming the AuNP is a sphere, $S_{\mathrm{AuNP(cps)}} = N_{\mathrm{AuNP(cps)}} \times \pi {d_{\mathrm{p,0}}}^2$. $N_{\mathrm{AuNP(cps)}}$ is the number of AuNPs delivered to the ICP-MS, and can be quantified using eqn (2) (details of the calibration methods are described in our previous work):[22]

$$N_{\mathrm{AuNP(cps)}} = \frac{N_{\mathrm{Au(cps)}} \times M_{\mathrm{m,Au}}}{6 \times 10^{23}} \times \frac{1}{V_{\mathrm{AuNP}} \times \rho_{\mathrm{Au}}}, \quad (2)$$

where $M_{\mathrm{m,Au}}$ and ρ_{Au} are the molecular mass and density of Au, respectively. V_{AuNP} is the volume of a AuNP ($= \pi {d_{\mathrm{p,0}}}^3/6$). A relative standard uncertainty of 7% is estimated for mass distribution measurements obtained in coupled mode; this value is based on the mean standard deviation performed at each size step.[22]

3 Results and discussion

3.1 Characterization of particle size distribution and colloidal stability

Fig. 2a shows the number-based PSD of AuNPs conjugated with TA-G1, G1-SH, and G2-COOH. The peaks located at ≈(4 to 6) nm for all samples are attributed to the salt residue particles generated by the electrospray process,[23] whereas peaks located at ≈(10 to 14) nm represent the population of singlet AuNPs (enlarged in Fig. 2b). By comparison to $d_{\mathrm{p,m}}$ of unconjugated AuNPs (11.1 nm for singlet), we found $d_{\mathrm{p,m}}$ of singlet AuNPs increases after dendron conjugation: *viz.* 12.2 nm for TA-G1–AuNP, 12.1 nm for G1-SH–AuNP, and 12.7 nm for G2-COOH–AuNP. The increase of $d_{\mathrm{p,m}}$ indicates the formation of a dendron corona on the surface of AuNPs. We note that the presence of AuNP aggregates (*i.e.*, peaks with $d_{\mathrm{p,m}}$ > 14 nm), apparent in Fig. 2a, are induced by the centrifugation cleaning process, during which the particles are forced into close contact. In this context, G2-COOH–AuNP contains a greater number of aggregates relative to G1-SH–AuNP and TA-G1–AuNP, most likely due to the lower surface packing of dendron ligands reported in our previous publication.[19]

Fig. 2c shows the PSD of the dendron–AuNPs after cisplatin complexation. For Pt^{II}-complexed G1-SH–AuNP and G2-COOH–AuNP (denoted as Pt^{II}–G1-SH–AuNP and Pt^{II}–G2-COOH–AuNP, respectively), the AuNP peak size occurs at ≈27 nm with a broad PSD. Compared with results in Fig. 2b (*i.e.*, without Pt^{II}), the increase of $d_{\mathrm{p,m}}$ from 13 nm to 27 nm shows evidence for aggregation induced by cisplatin complexation. Because the surface charge from the dendron conjugates (due to deprotonated carboxylic groups) is neutralized after complexing with Pt^{II}, electrostatic repulsion between particles decreases. In the absence of additional stabilizing factors (*e.g.*, steric hindrance), the colloidal stability of these dendron–AuNP constructs is decreased by Pt^{II}-complexation, leading to incipient aggregation. By comparison, the TA-G1–AuNP conjugate provides better colloidal stability after complexation (less aggregated) relative to G1-SH–AuNP or G2-COOH–AuNP. As shown in Fig. 2c, we observed several distinct peaks between $d_{\mathrm{p,m}}$ = 13 nm and $d_{\mathrm{p,m}}$ = 25 nm, which are attributed to the formation of discrete size AuNP clusters (GNCs).[15,24,25] The differences in colloidal stability observed for these samples can be attributed to a combination of several factors, including steric hindrance, ligand packing density, and also the extent of neutralization by Pt^{II}. The TA-G1–AuNP conjugate exhibits the greatest colloidal stability among the three species, possibly because of a sufficiently high surface ligand density,[19] with the least Pt^{II}-neutralization (discussed in a later section). Details of the identification of these GNCs will be described in the next section. The $d_{\mathrm{p,m}}$ of salt peaks for the cisplatin complexed species increases to ≈(8 to 10) nm, because additional nonvolatile salts (Na^+, Cl^-, Pt^{II}) are introduced during the ion-complexation process.

To reduce the interference from the salt peak in the PSD of Fig. 2c, we performed one cycle of centrifuge cleaning (*i.e.*, moderate centrifugation and replacement of supernatant with 4 mmol L^{-1} ammonium acetate solution) for all Pt^{II}–dendron–AuNP

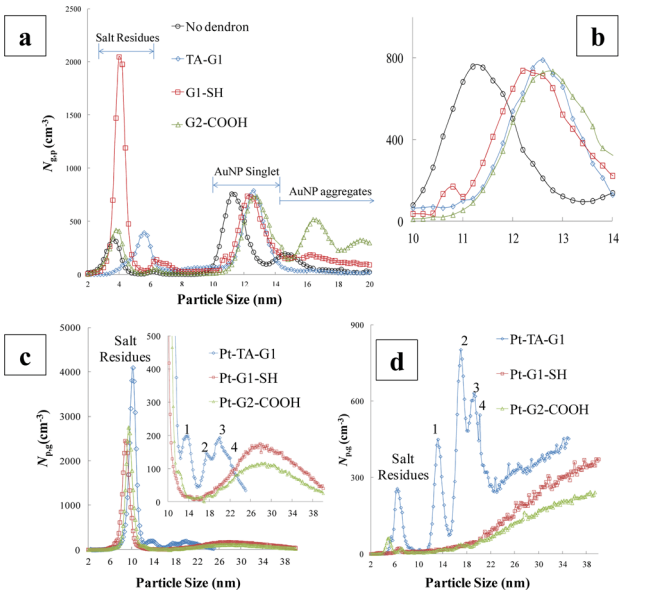

Fig. 2 Analysis of number-based PSD for dendron–AuNPs using ES-DMA-CPC. (a) Before Pt^{II} complexation. (b) Magnified regime representing AuNP singlet shown in (a). (c) After Pt^{II} complexation; dialysis without further cleaning. (d) After Pt^{II} complexation; dialysis plus one cycle of centrifugation cleaning.

samples. As shown in Fig. 2d, both the intensity and $d_{p,m}$ of salt residue peaks decreased after centrifugation cleaning. For the sample Pt^{II}–TA-G1–AuNP, the PSD of monomers (singlets), dimers, trimers, and tetramers become more distinguishable post-cleaning. The $d_{p,m}$ for singlet AuNPs increased by 0.5 nm, showing the addition of cisplatin slightly increases the cross-sectional area of the dendron corona. We note again that, the centrifugation cleaning process results in the formation of larger (less discrete sized) aggregates for cisplatin complexed conjugates, just as it did for the Pt^{II}–free dendron–AuNP conjugates. As a result of the reduced colloidal stability for both G1-SH–AuNP and G2-COOH–AuNP, the peak $d_{p,m}$ for these two samples became broadened and undifferentiated following centrifugation cleaning (*i.e.*, $d_{p,m} > 40$ nm).

After characterizing populations of AuNPs in the aerosol phase, we couple ICP-MS as a downstream detector and monitor the mass signals for ^{197}Au and ^{195}Pt *versus* the stepping of applied voltage in the DMA (*i.e.*, intensity of ^{197}Au and ^{195}Pt *versus* the selected $d_{p,m}$ during scanning). We focus solely on Pt^{II}–TA-G1–AuNPs in the main text and defer the results for Pt^{II}–G1-SH–AuNPs and Pt^{II}–G2-COOH–AuNPs to the ESI.† As shown in Fig. 3a, a peak at ≈9.6 nm was observed in the ^{195}Pt trace but not in the ^{197}Au trace, confirming the presence of ES-generated salt particles (identified as salt peaks in Fig. 2) that contain a measurable quantity of Pt^{II}. Except for the salt peak, the ^{195}Pt-trace closely follows the ^{197}Au-trace, indicating that most of the ^{195}Pt is associated with the Pt^{II}–dendron–AuNP conjugate (*i.e.*, not unbound ^{195}Pt in the solution phase). The centrifuge-cleaned sample shows the same trend: the ^{195}Pt and ^{197}Au traces are identical, confirming the results of Fig. 3a: the detected ^{195}Pt is principally associated with the dendron–AuNP conjugate through ion-complexation. As shown in Fig. 3b, the peak positions for ^{197}Au and ^{195}Pt traces are consistent with results obtained by ES-DMA-CPC (Fig. 2d), except the salt peak is not quantifiable by ES-DMA-ICP-MS (*i.e.*, the amount of ^{195}Pt is too low to be detected in the population of salt residue aerosol particles).

3.2 Identities and conformation of gold nanoparticle clusters

In the previous section (Fig. 2 and 3), we observed several distinct peaks from 12 nm to 25 nm for Pt^{II}–TA-G1–AuNP. These peaks can be attributed to discrete GNCs having specific numbers of primary AuNPs per cluster, and have been previously identified orthogonally by *ex situ* microscopic methods.[15,24] Based on the results of Fig. 2d and 3b, we calculated the relative mass M for each GNC, where $M = I/I_{N=1}$, and I is the center (maximum) intensity of the peak for the traced element at each specific peak, and $I_{N=1}$ is I for the singlet AuNP peak. If, as a first approximation, the mass of each primary particle is assumed to be identical, and the amount of ^{195}Pt is only dependent on the surface area of AuNPs, M will correspond to the average number of primary particles per cluster and can be quantified using both ^{197}Au and ^{195}Pt ICP-MS traces. Presumably Peak 1 contains only singlet AuNPs with $M = 1$; then $M = 2.0 \pm 0.1$ for Peak 2, $M = 3.0 \pm 0.1$ for Peak 3, and $M = 3.6 \pm 0.3$ for Peak 4 (summarized in Fig. 4a; The mean values reported are determined as the average of M (by ^{195}Pt) and M (by ^{197}Au), and the uncertainty is defined as one standard deviation of the mean value.). The results indicate good separation for Peak 2 (dimers) and Peak 3 (trimers), while a deviation was found for Peak 4 (*i.e.*, less than the value expected for a tetramer, $M \approx 4$). The major reason for this deviation is due to

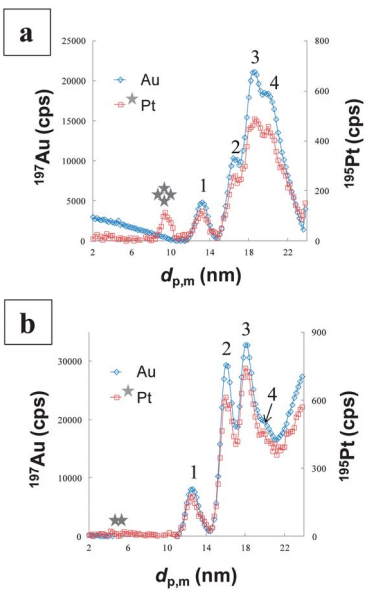

Fig. 3 Elemental-based PSD for Pt^{II}–TA-G1–AuNPs obtained in coupled mode using ES-DMA-ICP-MS. (a) Dialysis cleaning only. (b) Dialysis plus one cycle of centrifugation cleaning. Diamonds (blue): ^{197}Au trace; squares (red): ^{195}Pt trace.

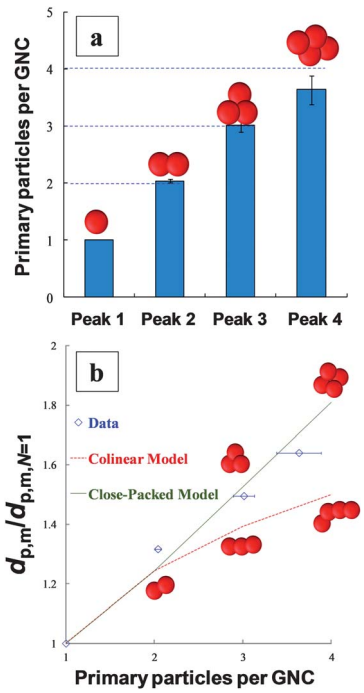

Fig. 4 Analysis of AuNP clusters (GNCs). (a) Number of primary AuNPs (or the average mass, M) per GNC, *versus* the peak number from Fig. 3. Blue dotted lines are to guide the eyes. (b) Normalized $d_{p,m}$ *versus* the number of primary particles per cluster. Sample: Pt^{II}–TA-G1–AuNP. Lines are to guide the eyes.

the decrease of resolution in the size separation with the increase of overlapping peaks, where Peak 4 probably contains trimers, tetramers and possibly a small number of pentamers (*i.e.*, less close to a pure tetramer peak in total population). Additionally, the higher order aggregates can exhibit a greater number of structural configurations, which in turn contribute to peak broadening. It is worth noting that the method proposed here can be particularly useful in characterizing samples containing overlapping peaks with similar or identical $d_{p,m}$, but characterized by different particle masses. For example, $d_{p,m}$ of bovine serum albumin-conjugated AuNP (BSA–AuNP) would be close to the value for the unconjugated AuNP dimer, if $d_{p,m}$ for bare AuNPs (monomers) is $\approx$13 nm.[25] Because M for a dimer AuNP is $\approx 2\times$ that for BSA–AuNP singlets, we can distinguish these two species using ES-DMA-ICP-MS.

Based on a free rotation model and knowing M for the GNCs, we can identify the conformation of GNCs classified by ES-DMA *versus* their normalized mobility size, $d_{p,m}/d_{p,m,N=1}$, where $d_{p,m,N=1}$ is $d_{p,m}$ for the singlet AuNP.[15,24,25] Fig. 4b shows the data for $d_{p,m}/d_{p,m,N=1}$ *versus* M in comparison with the two correlation fits, by assuming a close-packed (long dash, green) or a collinear structure (dotted line, red).[15] Our experimental data (diamonds) are consistent with the close-packed conformation, and the results are also consistent with our previous observation using *ex situ* transmission electron microscope.[15,24] In comparison, the GNCs separated by a liquid phase method (*e.g.*, field flow fractionation) are shown to be less close-packed (*i.e.*, a mixture of collinear and close-packed structures).[25] Hence our results suggest that the capillary force in play during the ES-drying process is sufficient to collapse the constituent particles into a close packed structure.[15]

3.3 Quantitative analysis of cisplatin loading on AuNPs

After identifying the GNC species present in the Pt^{II}–dendron–AuNP conjugate system, we can then quantify the loading of Pt^{II} for each species in terms of σ_{Pt}. As described in Section 2.2, σ_{Pt} can be represented as a function of the measured ^{195}Pt and ^{197}Au using ES-DMA-ICP-MS. As shown in Fig. 5a, σ_{Pt} is $\approx$2.7 nm^{-2} (1064 Pt^{II} molecules per AuNP) and $\approx$2.4 nm^{-2} (946 Pt^{II} molecules per AuNP), before and after centrifuge cleaning, respectively. We conclude from these results that σ_{Pt} is not dependent on the degree of aggregation of GNCs, indicating the Pt^{II}-complexation process (ion coupling to the dendron–AuNP conjugate) is much faster than the incipient aggregation of the Pt^{II}–dendron–AuNP product. Hence the mechanism of Pt^{II}-induced aggregation can be explained by standard colloidal stability theory: after Pt^{II} neutralizes the charge sites on TA-G1 under steady state conditions (*i.e.*, constant σ_{Pt}), the decrease of electrostatic repulsion reduces the energy barrier that prevents particle aggregation.

The remaining issue to address is the relationship between the dendron structure and the cisplatin loading. As shown in Fig. 5b, for the same starting concentration of Pt^{II}, σ_{Pt} was (2.4 $\pm$ 0.1) nm^{-2}, (3.0 $\pm$ 0.1) nm^{-2} and (3.4 $\pm$ 0.1) nm^{-2}, for TA-G1–AuNP, G2-COOH–AuNP and G1-SH–AuNP, respectively. The mean and uncertainty values for σ_{Pt} were derived from the

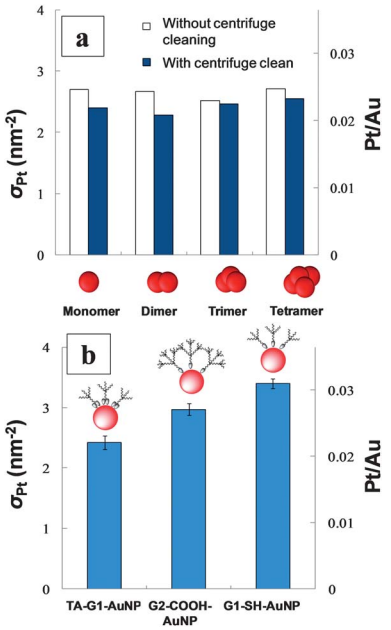

Fig. 5 Analysis of Pt^{II} loading on dendron–AuNP conjugates. (a) σ_{Pt} (left side ordinate) and Pt/Au (right side ordinate) of GNCs having different degrees of aggregation for the conjugate Pt^{II}–TA-G1–AuNP. (b) σ_{Pt} and Pt/Au ratio for three different dendron–AuNP conjugates. Samples were first dialyzed and then cleaned using a single cycle of centrifugation–resuspension.

average value of Pt/Au across a range of particle sizes in the mass-based PSD (details are described in the SI). The loading of Pt^{II} therefore increases with the number of available carboxyl sites for Pt^{II} complexation. Based on the XPS results measured previously,[19] the surface densities of carboxylic groups are 6.4 nm^{-2}, 7.9 nm^{-2} and 10.5 nm^{-2}, for TA-G1–AuNP, G2-COOH–AuNP and G1-SH–AuNP, respectively (details of this calculation are also provided in the SI). Assuming each Pt^{II} can bind with two carboxylic groups, the available sites for Pt^{II}-complexation (*i.e.*, theoretical maximum σ_{Pt}) are estimated to be 3.4 nm^{-2}, 4.0 nm^{-2} and 5.3 nm^{-2}, for TA-G1–AuNP, G2-COOH–AuNP and G1-SH–AuNP, respectively. As G1-SH–AuNP contains the most available carboxyl groups, σ_{Pt} should reach the highest level, and this is confirmed by our results. Though using G1-SH provides the highest Pt^{II}-loading, a significant trade-off must be made with respect to colloidal stability. We find that TA-G1–AuNPs exhibit better colloidal stability compared with G1-SH–AuNP, even though a higher percentage of its carboxyl groups were occupied by Pt^{II} molecules (*i.e.*, 76% for TA-G1–AuNP *versus* 65% for G1-SH–AuNP). Our results also indicate that G2-COOH may be insufficient to provide the required steric hindrance for the support of colloidal stability, in spite of its bulkier structure. Future studies will seek to incorporate a long-chain hydrophilic carboxyl-containing ligand with the short chain dendron moiety, in order to improve colloidal stability without compromising the capacity for high density loading of Pt^{II}.

4 Conclusions

A methodology based on coupling of ES-DMA with ICP-MS was applied to quantitatively determine the size-resolved cisplatin

loading for a model dendron-conjugated AuNP-based cancer therapeutic agent. Conjugation of dendron ligands, and the subsequent cisplatin complexation onto the conjugates, was monitored and characterized *via* changes in the physical size and elemental composition measured by ES-DMA-CPC and ES-DMA-ICP-MS, respectively. Surface loading of the cisplatin drug and colloidal stability of the drug-loaded conjugate, two key material properties for therapeutic performance, can be quantified through gas phase particle mobility classification with elemental detection. With the additional capability of resolving discrete size clusters formed during the complexation procedure, and determining the average mass per cluster by ICP-MS, we can accurately identify the cluster species (*i.e.*, dimers, trimers) and determine the drug loading for each. Our results also confirm that conformation of clusters is close-packed (as opposed to collinear) as a result of the ES-DMA aerosolization process. Importantly, the surface density of cisplatin is independent of the degree of aggregation of the clusters. Among three dendron–AuNP conjugates studied, TA-G1–AuNP shows the best colloidal stability, but the least cisplatin-loading. Our work provides proof of concept for application of coupled instrumentation (ES-DMA-ICP-MS) to quantify the surface density of functional molecular species on nanoparticles as a function of particle size.

Acknowledgements

This research was performed while S.E. held a National Research Council Research Associateship Award at NIST. The authors thank Drs Mindong Li and Yonggao Yan at NIST for their help with developing the customized DMA control program. The authors thank Drs Richard Gates, Michael Zachariah, Michael Winchester, Lee Yu, Robert Cook, Jingyu Liu, and Sang Min Lee at NIST for helpful discussions and manuscript review.

Notes and references

1 S. D. Brown, P. Nativo, J.-A. Smith, D. Stirling, P. R. Edwards, B. Venugopal, D. J. Flint, J. A. Plumb, D. Graham and N. J. Wheate, *J. Am. Chem. Soc.*, 2010, **132**, 4678–4684.
2 S. M. Lee, D. H. Tsai, V. A. Hackley, M. W. Brechbiel and R. F. Cook, *Nanoscale*, 2013, DOI: 10.10391/c3nr00333g.
3 P. G. Rose, *Nat. Rev. Clin. Oncol.*, 2011, **8**, 388–390.
4 T. Y. Seiwert, J. K. Salama and E. E. Vokes, *Nat. Clin. Pract. Oncol.*, 2007, **4**, 86–100.
5 M. E. Davis, Z. Chen and D. M. Shin, *Nat. Rev. Drug Discovery*, 2008, **7**, 771–782.
6 M. A. Dobrovolskaia and S. E. Mcneil, *Nat. Nanotechnol.*, 2007, **2**, 469–478.
7 J. B. Hall, M. A. Dobrovolskaia, A. K. Patri and S. E. McNeil, *Nanomedicine*, 2007, **2**, 789–803.
8 M. A. Dobrovolskaia, P. Aggarwal, J. B. Hall and S. E. McNeil, *Mol. Pharmaceutics*, 2008, **5**, 487–495.
9 J.-S. Lee, J. J. Green, K. T. Love, J. Sunshine, R. Langer and D. G. Anderson, *Nano Lett.*, 2009, **9**, 2402–2406.
10 J. V. Jokerst, T. Lobovkina, R. N. Zare and S. S. Gambhir, *Nanomedicine*, 2011, **6**, 715–728.
11 S. E. McNeil, *Characterization of Nanoparticles Intended for Drug Delivery*, Springer, New York, 2011.
12 D. H. Tsai, S. Elzey, F. W. DelRio, A. M. Keene, K. M. Tyner, J. D. Clogston, R. I. MacCuspie, S. Guha, M. R. Zachariah and V. A. Hackley, *Nanoscale*, 2012, **4**, 3208–3217.
13 J. D. Carter, N. N. Cheng, Y. Q. Qu, G. D. Suarez and T. Guo, *J. Phys. Chem. B*, 2007, **111**, 11622–11625.
14 A. K. Pradhan, S. N. Nahar, M. Montenegro, Y. Yu, H. L. Zhang, C. Sur, M. Mrozik and R. M. Pitzer, *J. Phys. Chem. A*, 2009, **113**, 12356–12363.
15 L. F. Pease, D. H. Tsai, J. L. Hertz, R. A. Zangmeister, M. R. Zachariah and M. J. Tarlov, *Langmuir*, 2010, **26**, 11384–11390.
16 J. I. Paez, E. A. Coronado and M. C. Strumia, *J. Colloid Interface Sci.*, 2012, **384**, 10–21.
17 W. E. Ghann, O. Aras, T. Fleiter and M. C. Daniel, *Langmuir*, 2012, **28**, 10398–10408.
18 M. C. Daniel, M. E. Grow, H. M. Pan, M. Bednarek, W. E. Ghann, K. Zabetakis and J. Cornish, *New J. Chem.*, 2011, **35**, 2366–2374.
19 T. J. Cho, R. A. Zangmeister, R. I. MacCuspie, A. K. Patri and V. A. Hackley, *Chem. Mater.*, 2011, **23**, 2665–2676.
20 M. C. Daniel and D. Astruc, *Chem. Rev.*, 2004, **104**, 293–346.
21 G. R. Newkome, C. N. Moorefield and F. Vötle, *Dendrimers and Dendrons: Concepts, Syntheses, Applications*, 2004.
22 S. Elzey, D. H. Tsai, L. Yu, M. W. Winchester, M. Kelly and V. A. Hackley, *Anal. Bioanal. Chem.*, 2013, **405**, 2279–2288.
23 D. H. Tsai, R. A. Zangmeister, L. F. Pease, M. J. Tarlov and M. R. Zachariah, *Langmuir*, 2008, **24**, 8483–8490.
24 D. H. Tsai, L. F. Pease, R. A. Zangmeister, M. J. Tarlov and M. R. Zachariah, *Langmuir*, 2009, **25**, 140–146.
25 D. H. Tsai, T. J. Cho, F. W. DelRio, J. Taurozzi, M. R. Zachariah and V. A. Hackley, *J. Am. Chem. Soc.*, 2011, **133**, 8884–8887.